

PARTICLE SIZE EFFECT ON MAGNETIC AND TRANSPORT PROPERTIES OF $\text{La}_{0.7}\text{Ca}_{0.3}\text{MnO}_3$ NANOPARTICLES

S. QASEEM, *K. MAAZ¹, A. MUMTAZ and S.K.HASANAIN

Department of Physics, Quaid-i-Azam University, Islamabad, Pakistan

¹Physics Division, Directorate of Science, PINSTECH, P.O. Nilore, Islamabad, Pakistan

(Received February 19, 2010 and accepted in revised form May 03, 2010)

$\text{La}_{0.7}\text{Ca}_{0.3}\text{MnO}_3$ nanoparticles have been synthesized by modified citrate route with particle sizes of 20, 26 and 32 \pm 3 nm respectively. The structural characterization has been performed by XRD and TEM analyses while magnetic characterization has been performed by vibrating sample magnetometer (VSM). This work presents the study of size effects on magnetic and electrical properties of Ca-doped CMR nanoparticles ($\text{La}_{0.7}\text{Ca}_{0.3}\text{MnO}_3$). Different particle sizes have been prepared by a wet chemical route. Magnetic characterization reveals that magnetization increases with the increase in the particle size and the magnetic transition temperature for larger particles is the same as in the bulk (258K). The ferromagnetic and resistive transitions are however broad compared to the case of bulk presumably due to the role of the surface. The metal-insulator transition temperature is found to be at 158K while the resistivity shows anomalous low temperature behavior with an upturn at low temperatures presumably due to coulomb blockade effects. Furthermore, the field dependence of the resistivity displays nonmonotonic behavior and is explained in terms of the field assisted tunneling between grains.

PACS: 73.23 Hk; 73.63 -b; 75.47 -m; 75.47 Gk. 75.75 +a

Keywords: Perovskite, Coulomb blockage, Electrical resistivity, Magnetic properties

1. Introduction

Perovskite type $\text{Ln}_{1-x}\text{A}_x\text{MnO}_3$ compounds where A represents divalent cations (such as Ca, Sr, or Ba) have been of interest for many years due to the discovery of the colossal magnetoresistance [1] at the hole doping concentration of (0.15<x<0.5). Colossal magnetoresistance (CMR) effects observed around the Curie temperature T_c [2] have made these materials a leading candidate for the application of magnetic sensors and reading heads. This family of compound shows further interesting electrical and magnetic characteristic when the grain or particle size reduces to nanometer scale due to the increase in the surface and inter-grain (-particle) effects [3,4]. Lopez-Qintela et al. [5] reported that the magnetization in $\text{La}_{0.7}\text{Ca}_{0.3}\text{MnO}_3$ increases as the particle size increases but the magnetic transition temperature (T_c) does not depend on the particle size, whereas K.Shanta [6] mentioned the dependence of T_c on particle size. The order of the ferromagnetic transition itself may be affected by the finite size of the particles and the incumbent changes in the electron hopping/tunneling between particles since

that may in turn affect the double exchange mechanism.

The electrical transport properties of CMR nanoparticle based systems also display interesting differences compared to the bulk and behave like a granular system that consists of small (nano) grains surrounded by insulating material. The electrostatic energy for the electron to hop from a charged to a neutral grain can be written as [7];

$$E_c = e^2/2C = e^2/4\pi \epsilon_0 d F(s/d) \quad (1)$$

Where e stands for electronic charge and C is the capacitance of the grain, ϵ_0 is the permittivity in vacuum, s is the grain separation, d is the grain diameter and the function F(s/d) depends on grain shape. From this equation it is obvious that E_c becomes very large for very small grain size (at the nanometer scale). Consequently for the small grains, as the temperature decreases it is increasingly difficult to activate the transport process and the situation may evolve to a point where the transport could be effectively blocked, known as coulomb blockade. For such situations

* Corresponding author : maaz@impcas.ac.cn

Sheng et al [8] suggested the temperature dependent conductivity behavior;

$$\sigma \propto \exp [-2(C/k_B T)^{1/2}] \quad (2)$$

whereas in order to explain the magnetotransport behavior for granular system two possible theoretical mechanisms have been proposed, viz spin dependent scattering between neighboring grains [9] and spin polarized tunneling [10]. Most of the recent reports of the magnetotransport effects in nanoparticles appear to support the latter hypothesis [11,12]. This latter model assumes the presence of a magnetic barrier between grains with misaligned spins that is reduced with increasing magnetic field (magnetization) and leads to increased conductivity. In general it has been suggested that two mechanisms contribute to the conductivity across the interparticle region, namely tunneling *through* the barrier and the thermally activated hopping *over* the barrier. Mitani et al. [13-15] proposed a model based on spin polarized tunneling influenced by the coulomb gap given as;

$$R_{\text{tunn}} \propto (1+P^2 m^2)^{-1} \exp (\Delta/T)^{1/2} \quad (3)$$

where P is the spin polarization, $m = M/M_s$ is the relative magnetization, and Δ is proportional to the coulomb charging energy and barrier thickness.

In this paper we report the preparation of $\text{La}_{0.7}\text{Ca}_{0.3}\text{MnO}_3$ nanoparticles and the study of their electrical and magnetic properties. The aim is to identify the differences in the behavior compared to the bulk behavior and the explanation of the same, based on the size, surface related and interparticle effects expected in an assembly of such particles, from the point of view of the size and interparticle effects and their consequences for the transition itself and the magnetotransport phenomenon.

2. Synthesis Technique

$\text{La}_{0.7}\text{Ca}_{0.3}\text{MnO}_3$ nanoparticles have been synthesized by modified citrate route [16]. The chemicals include: $\text{La}(\text{NO}_3)_3 \cdot 6\text{H}_2\text{O}$, $\text{Mn}(\text{NO}_3)_2 \cdot 4\text{H}_2\text{O}$, $\text{CaCl}_2 \cdot 2\text{H}_2\text{O}$ and anhydrous citric acid, all having purity upto 99.99%. We used the aqueous solution of the above salts in stoichiometric proportions. The pH was maintained at a level of 7 by adding concentrated NH_4OH solution and heating the mixture upto 80°C for 30 min. in order to complete the reaction. Finally cooled metal citrate solution was added to absolute ethanol

yielding the citrate precursor, which was given heat treatment, initially at 100°C then at 250°C for 6 hrs. and finally above 600°C to get the final product.

The structural characterization of the powder samples was performed using x-ray diffraction. The crystallite size was estimated by applying the Scherrer's equation as follows;

$$D = 57.3k\lambda/\beta\cos\theta \quad (4)$$

where k is the particle shape factor (generally taken as 0.9), λ is the wavelength of $\text{CuK}\alpha_1$ radiation (1.54\AA), β the calibrated half peak width of the selected diffraction peak, θ the Bragg angle (half of the peak position angle) and D the crystallite size. The average particle sizes that were annealed at 600 , 700 and 800°C , are found to be 20 , 26 and 32nm respectively with an error of $\pm 3\text{nm}$. TEM analysis for size determination yielded about 50nm average size for the particles annealed at 600°C as shown in Fig.1. The difference between the average particle size in the XRD and TEM is not unusual. It has been reported in [5, 17] that with the increase in the annealing temperature particles tend to agglomerate. TEM image gives the size of the agglomerated particles whereas x-ray diffraction pattern gives the crystallite size of the individual particles.

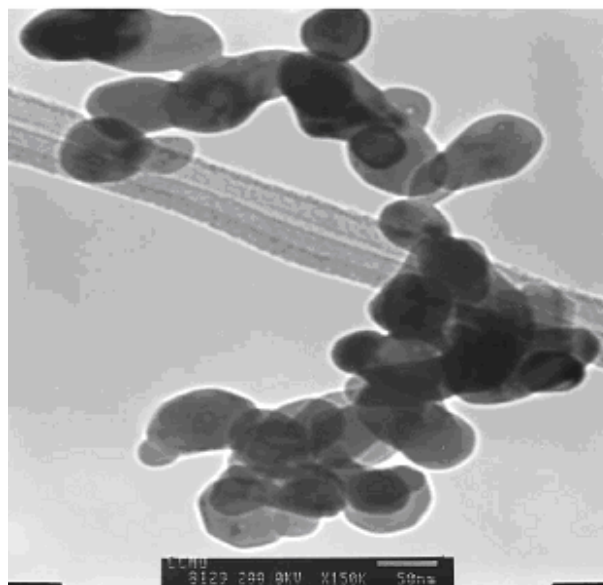


Figure 1. TEM image of $\text{La}_{0.7}\text{Ca}_{0.3}\text{MnO}_3$ nanoparticles annealed at 600°C . Average size is found to be 50nm .

3. Results and Discussion

The $\text{La}_{0.7}\text{Ca}_{0.3}\text{MnO}_3$ composition is well understood to be a ferromagnetic metallic below $T_c = 258\text{K}$ [18]. The magnetization as a function of temperature is shown in Fig. 2 for three different particle sizes. The critical temperature T_c was estimated from the point where the derivative of M vs T approached a maximum. It was observed that the transition temperature for the 26 and 32 nm particles was 258K similar to the bulk value [18].

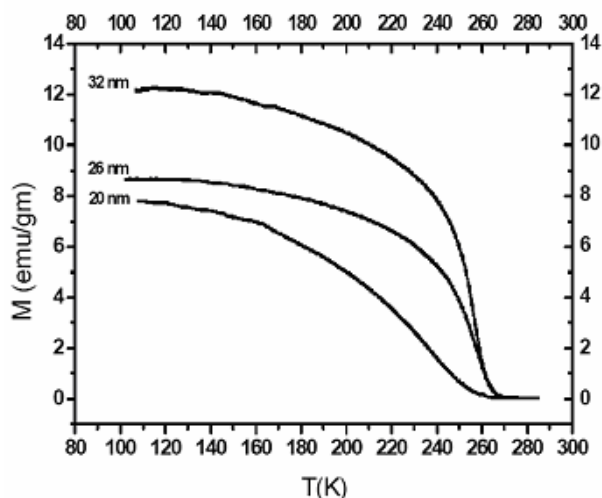


Figure 2. Field cooled $M(T)$ behavior showing increasing magnetization with decreasing particle size.

However, the transition temperature for the 20nm particles was found to be 240K suggesting that for smaller particle size (20nm) the finite size does lead to a significant lowering value of the T_c . It is also apparent that the 20nm particles have a much broader magnetic transition in comparison with the larger particles [5]. These effects find a simple explanation within the general picture of nanoparticles as comprising a core-shell structure [5] where the core (inner part) has a crystal structure with negligible defects while the shell (outer part) has numerous structural and bond defects. The spin misalignments in the shell hinder the interaction between the neighbouring grains or nanoparticles and the moments undergoes a more gradual transition as the temperature is lowered and the spin correlations build up. With decreasing particle size the effect of the surface (shell) becomes more dominant, leading to increased size effects for smaller size particles.

Saturation moments of the 20, 26 and 32nm particles at a field of 10kOe were determined from

the magnetization curves. It is observed that saturation moment increases with increasing particle size as shown in Fig. 3. This feature has also been reported earlier [5] and is in accordance with the core shell model for nanoparticles as discussed above.

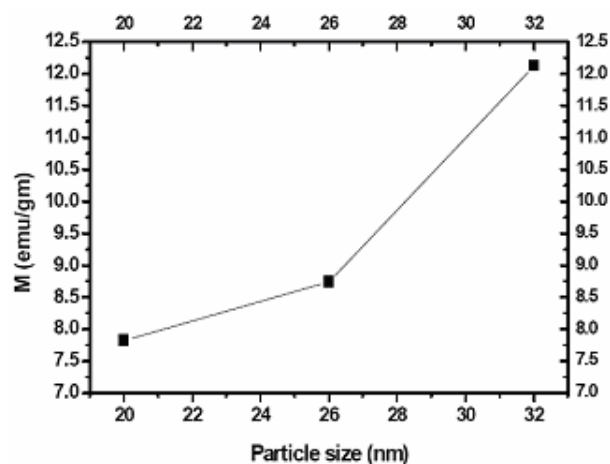


Figure 3. Saturation magnetization (M_s) as function of particle size (nm).

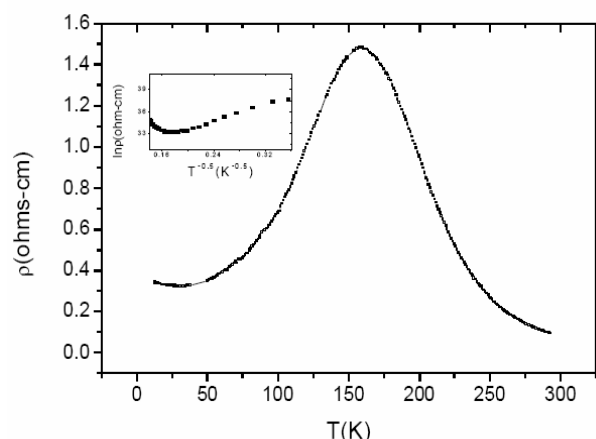


Figure 4. Resistivity behavior of 20nm particles as a function of temperature. Inset shows $\ln \rho$ has $T^{-1/2}$ dependence.

In order to measure the electrical resistivity we pelletized the 20 nm size particles under pressures of 400 kg-f/cm^2 and determined the resistivity by four probe method. Fig. 4 shows the resistivity behavior $\rho(T)$, for 20nm size particles in the absence of magnetic field. The insulator to metal transition temperature " T_{M-I} " was determined to be 158K from the peak of the resistivity. This T_{M-I} is very low compared to the magnetic transition temperature which was 240K for this case. In bulk materials, in contrast, T_c and T_{M-I} are found to be

nearly same [19] where increasing magnetic correlations help the transport in the Double Exchange model. This drastic difference in the electrical and magnetic transition temperatures has also been observed by others [3, 4]. A successful model to explain this behavior of nanoparticles has been proposed by Zhang et al. [20]. This model is based on the assumption of core shell structure of nanoparticles. Due to the presence of the defects in the shell (e.g. oxygen vacancies) and the spin misalignments therein, the transport of electrons is hindered between neighboring particles. Hence while individual particles maybe ferromagnetic and even metallic, the large intergrain resistivity dominates till much lower temperatures leading to low metal to insulator transition temperature (T_{M-I}).

The second important feature of resistivity is the slowing down of the decline and then the upturn in its value at low temperatures ($T < 40K$). This is shown in detail in the inset of Fig. 4, where $\ln \rho$ is plotted vs $T^{-1/2}$. The linear variation of $\ln \rho$ vs $T^{-1/2}$ is apparent for low temperatures. As discussed in the introduction that such temperature dependence of $\ln \rho$ is expected due to the presence coulomb barrier at the intergrain regions leading to a thermally activated form for ρ as suggested by eq. 2;

$$\rho \propto \exp[2(C/k_B T)^{1/2}] \quad (5)$$

We have also investigated the resistivity behavior in the presence of D.C magnetic field. The data is shown in Fig. 5, when the sample was cooled at 10K while an identical behavior was also observed for the $\rho(H)$ behavior at 50K. The resistivity is seen to start from a high value at $H = 0$ and begins to decrease with increasing field (path indicated as R_1 in the figure); in decreasing fields down to zero (path R_2) there is a significant hysteresis for low fields with the resistivity being lower than in the path R_1 . On crossing into the negative field region (R_3) the resistivity continues to rise upto $H=350Oe$ and thereafter decreases. The return path from the negative field maximum to zero (path R_4) has the same trend as in R_2 . Once again on crossing into the positive field values from zero (path R_5) there is a peak in the resistivity as in path R_3 . An understanding of this peak effect can be explained from looking at the typical magnetic hysteresis behavior (Fig. 6) at the lowest temperature accessible in the magnetometry experiment, 77K. The peaks in the resistivity

correspond to the regions where the remanent moment obtained after cycling from high fields declines to zero ($0, H < H_c$). The decline regions of resistivity vs field correspond to the field regions where the moment is increasing (whether in a positive or negative sense), while the hysteresis of $M(H)$ is reflected in the hysteresis in $\rho(H)$.

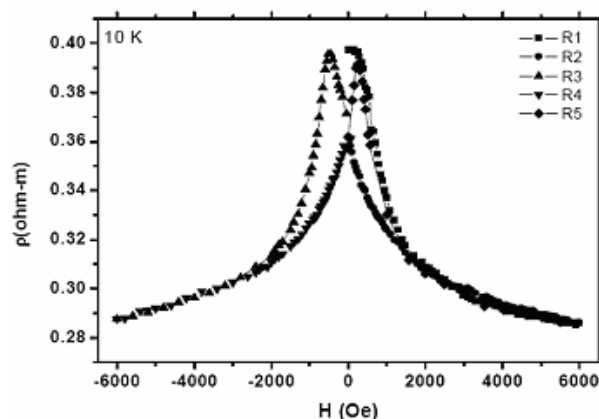


Figure 5. Field dependence of resistivity for 20nm particles at 10K. Paths indicated are as follows: R_1 increasing field; R_2 decreasing field; R_3 field increasing in negative direction; R_4 the return path from the negative; R_5 cycling again to positive field direction.

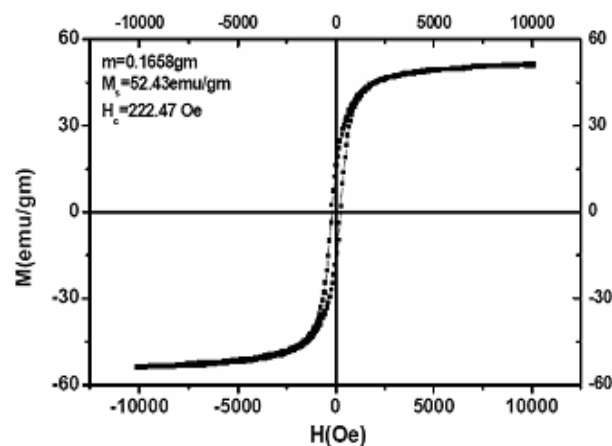


Figure 6. $M(H)$ Loop of 20nm particles at 77K and maximum field upto 10 kOe.

The low field magnetoresistance of the particles, defined as $[(\rho(0) - \rho(H))]/(\rho(0))$ is shown in Fig. 7 for a temperature of 50K. These sharp peaks at low fields (324Oe) are closely similar to the trend shown in [21, 22] for CrO_2 nanopowders and ultrathin films of manganites, respectively. While the high temperature and high field MR in CMR compounds is associated with the stabilization of the moment by the field and the consequent ease

of electron transport within the grains, the low temperature and low field effects have a different interpretation. These arise, as in Eq. 3, from the improved intergrain conductance due to the improved spin dependant tunneling when the field is increased. The number of antiparallel interparticle spin alignments peaks at the critical field H_c [21] leading to a large resistance as well as large magnetoresistance effects. The strong changes in the values of resistivity at very low fields suggest that there is a weak linkage between the neighboring particle moments so that the application of even small fields results in a major change in the resistivity values. The fields where the peaks are observed (324Oe) appear to fall reasonably close to where one may expect the coercivity to lie at this temperature considering that H_c at 77K is 222Oe and may be expected to increase further at lower temperature.

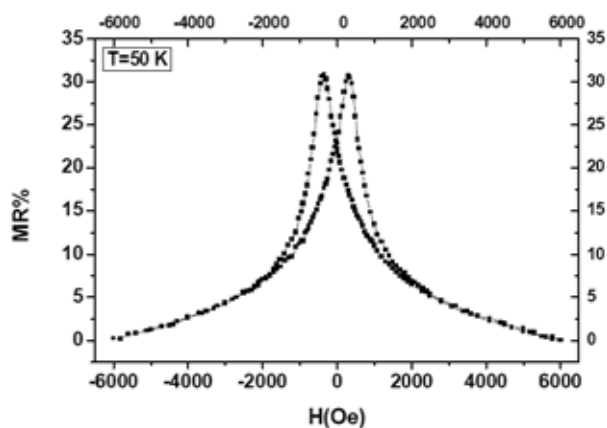


Figure 7. Field dependence of magnetoresistance of 20nm particle at 50K.

Comparison of the magnetoresistance effects at 50 and 10K is shown in Fig.7, where the zero field values refer to values obtained after decreasing the field to zero after exposing upto a high field i.e. in the remanent moment state. It is evident that at low fields the coulomb blockade effect is predominant and the resistivity values are higher for 10K than for 50K. However with increasing fields beyond the peak, the increasing M dominates and with increased hopping probability, the resistivity at 10K decreases to a value less than the corresponding value for 50K. Essentially the increased ease of spin alignment at 10K promotes the spin dependant tunneling to decrease the resistance faster than at 50K.

4. Conclusion

In conclusion we say that as the particle size decreases the surface to volume ratio increases and hence the surface effects become more pronounced for smaller particles. Nearly all of our results show the influence of surface effects on the electrical as well as magnetic properties and support the of core-shell model of our particles. The lack of a resistive continuity in the nanoparticles, due to the intergrain barriers may be one reason that the conduction processes, and hence the double exchange, do not show an abrupt change at the T_c where the ferromagnetic alignments become long range. Similarly the electrical properties of 20nm size particles show a clear signature of the coulomb blockade testifies that the conductance at low temperatures becomes dominated by the activation over these barriers. Also the decrease in metal to insulator transition temperature and study of low field magnetoresistance support the weak linkage between the particle moments due to surface disorder. It is also evident from the low field magnetoresistance studies that there is a spin dependant intergranular tunneling mechanism along with the coulomb barrier.

Acknowledgement

The authors acknowledge the Higher Education Commission of Pakistan (HEC) for providing financial support to perform this research work.

References

- [1] V. Helmot, J. Wecker, B. Holzapfel, L. Shultz and K. Samwe, Phys. Rev. Lett. **71**, No. 14 (1993) 2331.
- [2] W.E. Pickett and D.J. Singh, Phys. Rev. B **53**, No. 3 (1996) 1146 also C.N.R. Rao, R. Mahesh, A.K. Raychaudhuri and R. Mahendiran, J. Phys. Chem. Solids **59**, No. 4 (1998) 487.
- [3] F. Rivadualla, L.E. Hueso, J. Rivas, M.C. Blanco, M.A. Lopez-Quintela and R.D. Sanchez, J. Magn. and Magn. Materials **203** (1999) 253.
- [4] J. Rivas, L.E. Hueso, A. Fondado, F. Rivadualla and M.A. Lopez-Quintela, J. Magn. and Magn. Materials **221** (2000) 57.
- [5] M.A. Lopez-Quintela, L.E. Hueso, J. Rivas and F. Rivadulla, Nanotechnology **14** (2003) 212.

- [6] K. S. Shankar, S. Kar, G.N. Subbhanna and A.K. Raychaudhuri, *Solid State Communications* **129** (2004) 479.
- [7] M. Ziese, *Rep. Prog. Phys.* **65** (2002) 143.
- [8] P. Sheng, B. Abeles and Y. Arie, *Phys Rev. Lett.* **31** (1973) 44.
- [9] A. Gupta et al., *Phys. Rev. B* **54** (1996) 15629.
- [10] J. S. Helman and B. Abeles, *Phys. Rev. Lett.* **37** (1976) 1429.
- [11] Li. Balcells, J. Fontcuberta, B. Martinez and X. Obradors, *Phys. Rev. B* **58** (1998) 14697.
- [12] P. Raychaudhuri, K. Sheshadri, P. Taneja, S. Bandyopadhyay, P. Ayub, A.K. Nigam, R. Pinto, S. Chaudhary and S.B. Roy, *Phys. Rev. B* **59** (1999) 13919.
- [13] S. Mitani, S. Takahashi, K. Takanashi, K. Yakushiji, S. Maekawa and H. Fujimori, *Phys. Rev. Lett.* **81** (1998) 2799.
- [14] J. Inoue and S. Maekawa, *Phys. Rev. B* **53** (1996) R11 927.
- [15] T. Zhu and J. Wang, *Phys. Rev. B* **60**, No. 11 (1999) 918.
- [16] J.H. Choy, D.H. Kim, C.W. Kwon, S.J. Hwang and Y.I. Kim, *J. of Power Sources* **77** (1999) 1.
- [17] T. Yi, S. Gao, Xing Qi, Y. Zhu, F. Cheng, B. Ma, Y. Huang, C. Liao and C. Yan, *Journal of Physics and Chemistry of Solids* (2000) 1407.
- [18] X.X. Zhang, J. Tejada, Y. Xin, G.F. Sun, K.W. Wong and X. Bohigas, *Appl. Phys. Lett.* **69** (1996) 3596.
- [19] P. Schiffer, A.P. Ramirez, W. Bao and S.W. Cheong, *Phys. Rev. Lett.* **75** (1995) 3336.
- [20] N. Zhang, W. Ding, W. Zhong, D. Xing and Y. Du, *Phys. Rev. B*, **56** (1997) 8138.
- [21] J. Dai and J. Tang, *Phys. Rev. B* **63** (2001) 054434.
- [22] Wang et al. *Appl. Phys. Lett.* **74** (1999) 2212.